This is an open access article published under an ACS AuthorChoice License, which permits copying and redistribution of the article or any adaptations for non-commercial purposes.

Slippery Wenzel State

Xianming Dai, Birgitt Boschitsch Stogin, Shikuan Yang, and Tak-Sing Wong*

Department of Mechanical and Nuclear Engineering and Materials Research Institute, The Pennsylvania State University, University Park, Pennsylvania 16802, United States

ABSTRACT Enhancing the mobility of liquid droplets on rough surfaces is of great interest in industry, with applications ranging from condensation heat transfer to water harvesting to the prevention of icing and frosting. The mobility of a liquid droplet on a rough solid surface has long been associated with its wetting state. When liquid drops are sitting on the top of the solid textures and air is trapped underneath, they are in the Cassie state. When the drops impregnate the solid textures, they are in the Wenzel state. While the Cassie state has long been associated with high droplet mobility and the Wenzel state with droplet pinning, our work challenges this existing convention by showing that *both* Cassie *and* Wenzel state droplets can be highly mobile on nanotexture-enabled slippery rough surfaces. Our surfaces were developed by engineering hierachical nano- and microscale textures and infusing liquid lubricant into the nanotextures alone to create a highly slippery rough surface. We have shown that droplet mobility can be maintained even after the Cassie-to-Wenzel transition. Moreover, the discovery of the slippery Wenzel state allows us to assess the fundamental limits of the classical and recent Wenzel models at the highest experimental precision to date, which could not be achieved by any other conventional rough surface. Our results show that the classical Wenzel eq (1936) cannot predict the wetting behaviors of highly wetting liquids in the Wenzel state.

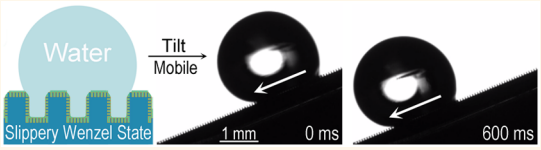

KEYWORDS: Wenzel state · Cassie state · wetting · droplet mobility · slippery rough surface

Maintaining high droplet mobility on rough surfaces is of great interest in many industrial applications.[1−8] The mobility of liquid droplets on these rough solid surfaces is highly dependent on how liquids wet the surface textures. The notion that liquid droplets are mobile in the Cassie state and pinned in the Wenzel state has been deeply rooted in the field of wetting for more than a decade.[1,2,4,9,10] Drop mobility on a surface is strongly influenced by contact line pinning,[11−13] which originates at the nanoscale.[14] The degree of contact line pinning is quantified by contact angle (CA) hysteresis ($\Delta\theta^*$) − the difference between the advancing apparent CA (θ_A^*) and receding apparent CA (θ_R^*). On conventional rough substrates, the CA hysteresis of a Cassie droplet is much smaller than its apparent CA, θ^* (*i.e.*, $\theta^* \gg \Delta\theta^*$), and the CA hysteresis of a Wenzel droplet is typically on the same order of magnitude of its apparent CA (*i.e.*, $\theta^* \sim \Delta\theta^*$).[4,9]

Because of this fundamental difference, there are a number of scientific and technological challenges associated with Wenzel state droplets. Scientifically, a large $\Delta\theta^*$ value is associated with large uncertainty in apparent CA measurements.[4,9] Thus, precise experimental validation of the classical Wenzel eq (1936)[1] has remained an open scientific question for the past 79 years. Technologically, sustaining a droplet in the Cassie state is difficult, as the air layer underneath the droplets can be disrupted when subjected to high pressure,[15] high temperature,[16] liquids with low surface tension,[3,17] or when encountering liquids with impurities. Moreover, condensation from microscopic liquid drops will fully impregnate surface textures, making it extremely challenging, and often impossible, to maintain droplets in the Cassie state in industrial applications such as fog harvesting,[18] dropwise condensation,[19,20] and ice prevention.[21] In an effort to recover droplet mobility, previous research studies have been predominantly focused on inducing Wenzel-to-Cassie transition. Thus far very few design strategies can restore the liquid from the Wenzel state to the Cassie state, and strategies successful in doing so require the use of external energy.[22−24]

Here, we report a new phenomenon in which Wenzel state droplets exhibit high droplet mobility on rough microtextured surfaces with a conformal lubricant layer held in place by nanotextures. We have shown that droplet mobility can be retained even after the Cassie-to-Wenzel transition. These results contrast the conventional

* Address correspondence to tswong@psu.edu.

Received for review July 6, 2015 and accepted August 21, 2015.

Published online August 24, 2015
10.1021/acsnano.5b04151

© 2015 American Chemical Society

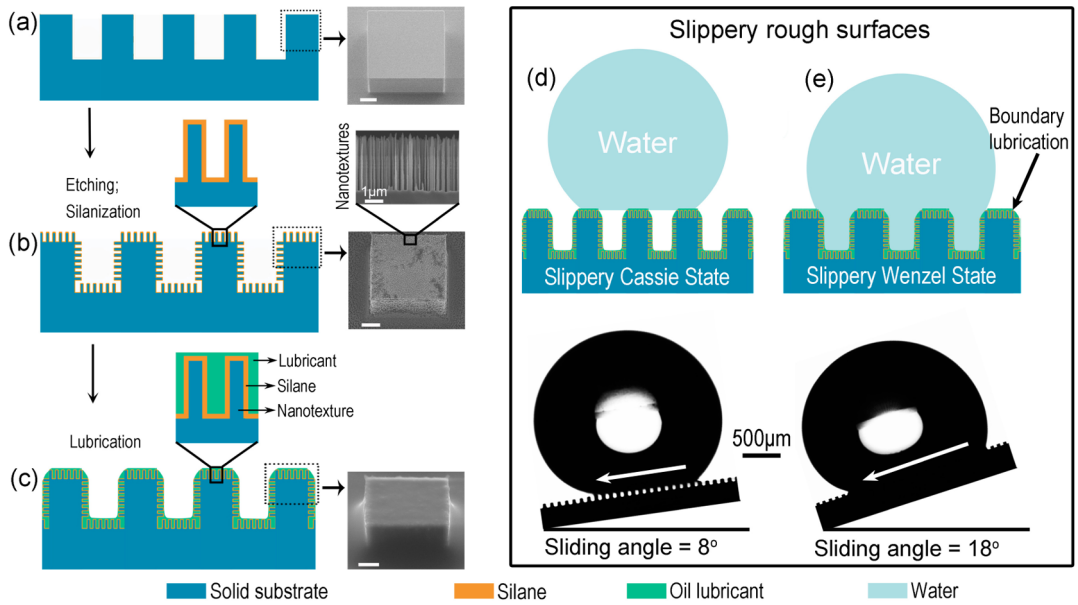

Figure 1. Fabrication of slippery rough surfaces and their liquid repellency in both Cassie and Wenzel states. (a) Silicon micropillars ($w = 50\ \mu$m, $L = 50\ \mu$m, $h = 20\ \mu$m). (b) Nanotextured and silanized silicon micropillars. (c) Slippery rough surfaces created by infusing lubricant into the nanotextures alone. (d) A Cassie state droplet on the slippery rough surfaces ($w = 50\ \mu$m, $L = 50\ \mu$m, $h = 50\ \mu$m). The sliding angle is 8°. (e) A slippery Wenzel state droplet on the slippery rough surface ($w = 47\ \mu$m, $L = 53\ \mu$m, $h = 19\ \mu$m) with the sliding angle of 18°. The drop volumes are 10 μL. Scale bars in panels a, b and c represent 10 μm.

concept that Cassie drops are slippery and Wenzel drops are sticky. Furthermore, we have demonstrated that, due to their low CA hysteresis, these slippery rough surfaces allow for more precise quantitative validation of the Wenzel wetting models. Specifically, they allow for the most precise measurement of apparent contact angles known to date, enabling them to serve as the state-of-the-art materials systems for assessing the accuracy of theoretical CA predictions and the fundamental limits of these theoretical models.

RESULTS AND DISCUSSION

Design Rationale. The physical origin of Wenzel droplet immobility is pinning, which results from the interaction of the liquid contact line with chemically heterogeneous surfaces or micro/nanoscopic sharp edges of the surface textures.[11] Pinning can be minimized by creating chemically homogeneous and molecularly smooth surface textures with rounded edges,[12,25] but such an idealized rough surface is extremely challenging to manufacture even with the most advanced nanofabrication techniques. We hypothesize that by infusing a chemically homogeneous layer of lubricant into the nanotextures of a hierarchically structured surface comprised of micro- and nanoscale textures, the sharp edges can be smoothened by the liquid lubricant, yielding a conformally lubricated rough surface. The pinning effect on such surfaces could be greatly reduced,[11,12] and may lead to enhanced droplet mobility in both Wenzel and Cassie states (Figure 1).

Design and Fabrication. To create a slippery rough surface with a conformal lubricant layer, it is important that the lubricant layer must be thermodynamically stable. In addition, it must be energetically more favorable for the lubricants, rather than the immiscible foreign liquids, to wet the solid textures.[5,26] The first criterion can be satisfied by choosing a lubricant that can wet the solid, and by creating nanoscale textures on micropillars, forming hierarchical structures. To describe the surface roughness (defined as the ratio of the actual to the projected surface areas) of these dual length scale structures, we define R as the roughness resulting from the micropillars alone, and r as the roughness resulting from nanotextures alone (*i.e.*, r represents local roughness). The increased surface area due to roughness together with the chemical affinity between the substrate and the lubricant will enhance lubricant wetting. The second criterion can be satisfied by choosing an appropriate solid and lubricant combination for an immiscible foreign fluid such that the following relationships are satisfied:[5,26]

$$r(\gamma_B \cos\theta_B - \gamma_A \cos\theta_A) - \gamma_{AB} > 0$$

and

$$r(\gamma_B \cos\theta_B - \gamma_A \cos\theta_A) + \gamma_A - \gamma_B > 0 \qquad (1)$$

where γ_A and γ_B are, respectively, the surface tensions for the foreign liquid and for the lubricant; γ_{AB} is the interfacial tension between the foreign liquid and lubricant; θ_A and θ_B are the equilibrium contact angles for the foreign liquid and the lubricant on a given flat solid surface, respectively. These relationships dictate the solid-lubricant combinations and the required surface roughness to form an energetically stable lubricating

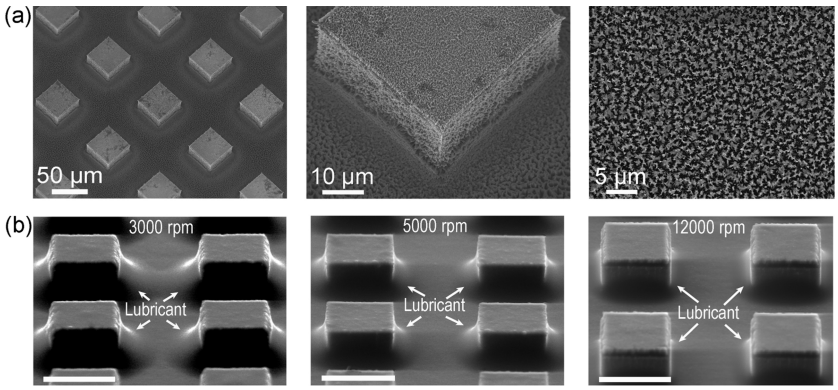

Figure 2. Characterization of the micropillars before and after lubrication. (a) Patterned nanotextured micropillars without lubrication. (b) Lubricant distribution on the lubricated micropillars at various spinning speeds. Scale bars represent 50 μm.

film within the nanotextures of the solid that will not be displaced by the external fluid (Supporting Information).

On the basis of these design criteria, we used silicon as the substrate to create the slippery rough surfaces. Square-shaped micropillars of width w, interpillar spacing L, and height h were fabricated using photolithography and deep reactive-ion etching (Figure 1a), followed by a wet etching method to create nanostructures on the micropillars (Figure 1b). Because we were interested in the mobility of Wenzel state droplets, we carefully designed the geometrical parameters of the micropillars based on the following governing relationship to ensure that the Wenzel state was energetically more favorable than the Cassie state:[9]

$$\cos\theta_c = \frac{\Phi_s - 1}{R - \Phi_s} \quad (2)$$

Here, θ_c is the critical intrinsic CA below which Cassie-to-Wenzel transition is favorable; Φ_s is the solid fraction ($\Phi_s = w^2/(w + L)^2$). The surface roughness of the lubricated micropillars, R, is the ratio of geometric area and projected area and can be expressed as $R = 1 + 4wh/(w + L)^2$. Since the maximum liquid CA on a smooth surface is ~120°,[27] we designed the geometries of the surface textures such that $\theta_c > 120°$ to ensure that liquid droplets in the Wenzel state are more energetically favorable (note that metastable Cassie state could still be possible).[9]

We then chose perfluorinated silanes to functionalize the silicon hierarchical textures and perfluorinated oils (*i.e.*, DuPont Krytox oils—perfluoropolyether) for the lubrication since these lubricants are immiscible to both aqueous and nonaqueous phases (Figure 1c). The lubricant was applied onto the solid substrate by a spin-coating process, where excess lubricant was removed from the micropillar structures by a spin coater at high spin speed (Figure 2a, b). Because of the dominance of capillary force per unit volume at smaller length scales, the nanotextures retained the lubricant more favorably compared to the microscopic roughness.[28] In addition, the presence of the nanotextures on the micropillars greatly enhances lubricant retention against shedding of contacting fluid droplets. For example, the microstructured surface with lubricant-infused nanotextures can repel at least 200 water droplets with little change in droplet repellency, whereas the lubricated surface without nanotextures lost its liquid repellency after shedding only three water droplets (Supporting Information). The high roughness of the nanotextures and the strong chemical affinity of the silane coatings to the perfluorinated lubricant together allowed the lubricant to completely infuse the nanotextures, thus forming a conformal, chemically homogeneous lubricant layer over the micropillar structures (Supporting Information). Consequently, the slippery rough surface with conformal lubrication was obtained. Such a slippery rough surface enables high droplet mobility for both Wenzel (Supplementary Movie S1) and Cassie (Supplementary Movie S2) state droplets (Figure 1d,e).

Surface Morphology and Wetting Characterizations. To verify the surface homogeneity, we performed high resolution environmental scanning electron microscopy (ESEM) to visualize the surface morphologies before and after the lubrication of the nanotextures (Figure 3a,b). Before the lubrication, the substrate is rough at the nanoscale; after lubrication the surface is smooth at the nanoscale because the nanostructures are submerged beneath the liquid lubricant. Our high resolution ESEM image showed that the radius of curvature of the lubricated edge is ~4.2 μm ± 0.5 μm (*i.e.*, microscopic sharp edge) as compared to that of the nonlubricated surface textures which is <100 nm ± 10 nm (*i.e.*, nanoscopic sharp edge) (Figure 3a,b).

We quantified the surface retention behaviors of water droplets in different wetting states on the lubricated and nonlubricated rough surfaces. For a liquid droplet to move on a surface tilted at an angle α, the tangential component of the gravitational force, F_{gt}, acting on the droplet has to exceed the surface retention force, F. Specifically, the tangential gravitational

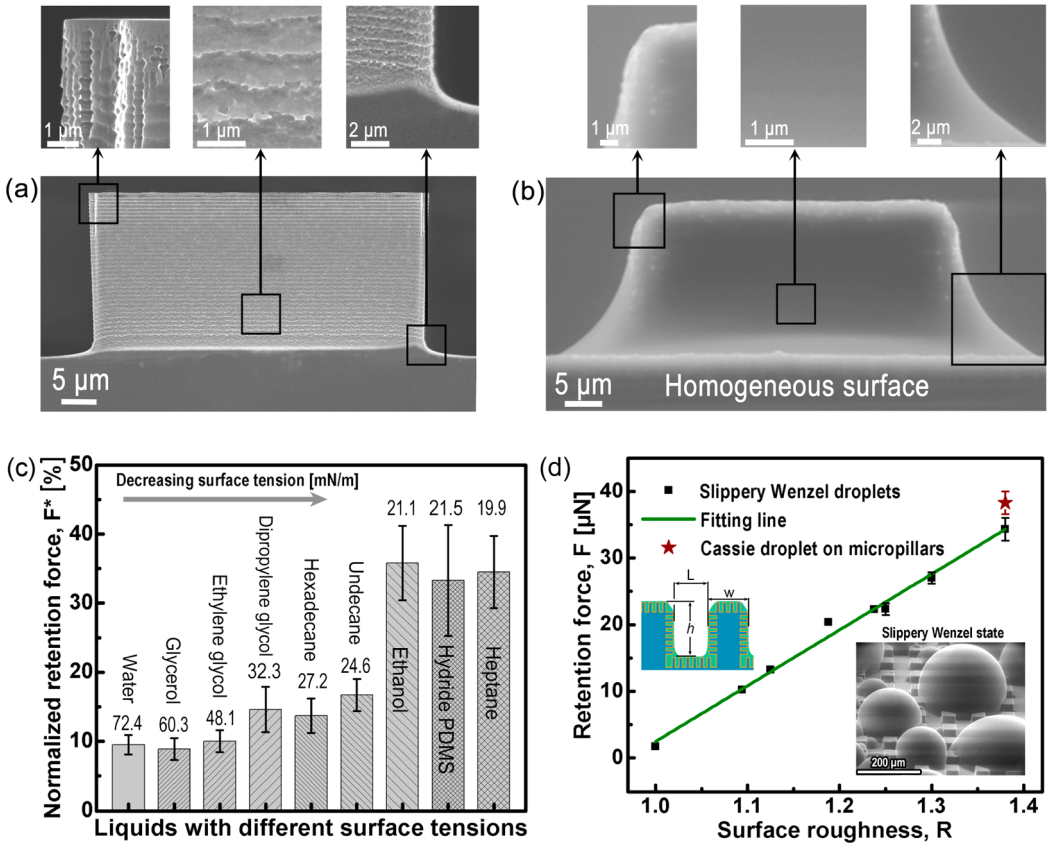

Figure 3. Comparison of surface morphology and pinning forces on nonlubricated and lubricated rough surfaces. (a) SEM image of a nonlubricated silicon micropillar with sharp corner (*i.e.*, small radius of curvature) and rough surface. (b) ESEM image of a lubricated micropillar with round corner (*i.e.*, large radius of curvature) and smooth surface. (c) Normalized retention force F^* of liquids with different surface tensions on lubricated rough surfaces of roughness $R = 1.38$. (d) Retention force F of liquid droplets on lubricated rough surfaces and superhydrophobic surfaces. F for a Cassie droplet is defined as the retention force of a Cassie droplet on nonlubricated micropillars without nanostructures ($w = L = 50$ μm, $h = 20$ μm). The coefficient of determination is 0.996 for the linear fit curve depicted here.

force and the surface retention force acting on the droplet can be respectively expressed as,[29]

$$F_{gt} = \rho V g \sin\alpha \quad \text{and} \quad F = \gamma D(\cos\theta_R^* - \cos\theta_A^*) \quad (3)$$

where ρ, γ, V, and D are the density, surface tension, volume, and wetting width of the liquid droplet, respectively; g is the acceleration due to gravity.

To quantify the force required to initiate the droplet motion, we gradually increase the tilting angle α until the water droplet begins to slide (*i.e.*, $F_{gt} = F$). We examined the droplet mobility of a broad range of aqueous and organic liquids with surface tensions ranging from ~72.4 mN/m to ~19.9 mN/m on the conformally lubricated rough surfaces (Figure 3c and Supplementary Movie S3). Specifically, the measured retention force F increases linearly with surface roughness R on lubricated surfaces (Figure 3d). Results show that the mobility of Wenzel droplets on the slippery rough surfaces is maintained even for liquids with low CAs. To compare the relative magnitude of the retention force on lubricated and nonlubricated substrates, we define F^* as the retention force of the Wenzel state droplet on lubricated micropillars normalized by that on nonlubricated ones without nanotextures and with the same micropillar geometries as their conformally lubricated counterparts. F^* ranges from ~10% for high surface tension (72.4 mN/m) fluids to ~36% for low surface tension (19.9 mN/m) fluids (Figure 3c).

The reduced pinning forces for the lubricated substrates are attributed to the smooth, rounded edges of the chemically homogeneous liquid-infused surface textures and the mobility of the lubricant surface (*i.e.*, liquid lubricant molecules can slide past one another). Pinning reduction due to increased edge radius of curvature is consistent with a classical study performed by Oliver *et al.*,[12] who demonstrated that a microscopic sharp edge has reduced liquid pinning strength compared to that of molecularly sharp edge. In addition, it has been shown that liquid-like surfaces exhibit negligible contact angle hysteresis due to the molecular smoothness and mobility.[5,30−32] Since our lubricated rough surface is conformally covered with a liquid lubricant, these molecularly mobile surfaces further reduce the resistance of liquid contact line motion as compared to a rigid solid surface. The synergistic effects of smoothened edges and the molecular

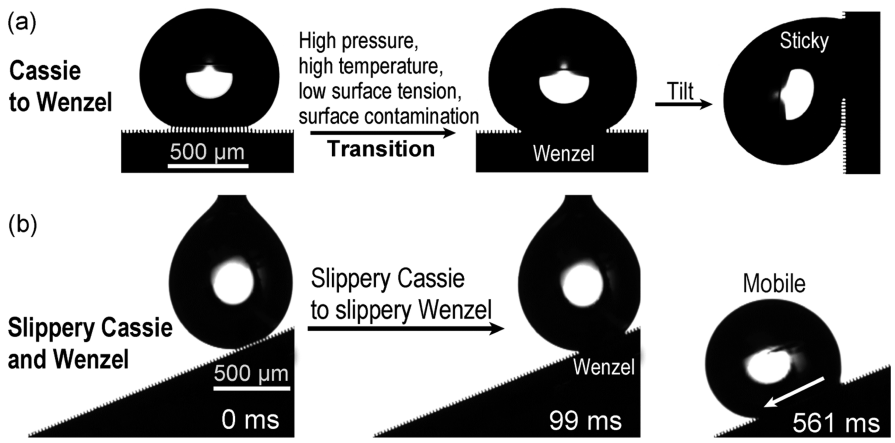

Figure 4. Droplet mobility on nonlubricated and lubricated rough surfaces. (a) Transition of a liquid droplet from the Cassie state to the Wenzel state on a silanized microstructured surface. The droplet is mobile in the Cassie state and sticky in the Wenzel state. (b) Transition of a liquid droplet from the Cassie state to the Wenzel state on a lubricated microstructured surface in which the nanotextures alone are infused with lubricant. The droplets are mobile in both the Cassie and Wenzel states. Note that the Cassie state is metastable.

mobility of the lubricant contribute to the observed slipperiness of Wenzel state droplets. These combined effects also lead to a surprising observation that the retention force of Wenzel droplets on the lubricated surface could be smaller than that of the Cassie droplet on a nonlubricated surface with the same solid fraction (Figure 3d).

Technological Significance: Liquid Repellency in both the Cassie and Wenzel States. Our experimental results demonstrate that lubricated rough surfaces are capable of maintaining droplet mobility regardless of wetting state. It is important to note that Cassie-to-Wenzel transition can be easily induced on any textured surfaces either by low surface tension fluids, by external pressure, or by contaminations (Figure 4a). Such a transition will eventually render the liquids immobile on nonlubricated rough surfaces. While tremendous efforts have been invested in preventing or delaying the transition to the Wenzel state,[3,8,33,34] our results show that one can circumvent this challenging issue altogether by simply coating a conformal layer of liquid lubricants on rough solid textures; doing so allows liquid droplets to maintain their mobility in both Cassie and Wenzel states (Figure 4b, Supplementary Movies S4 and S5). This could effectively circumvent the Wenzel-to-Cassie transition challenge, creating a simpler, passive method of maintaining drop mobility in both the Cassie and Wenzel states.

Scientific Significance: Validation of Classical and Recent Wenzel Wetting Models. With the identification of the slippery Wenzel state, we can now quantitatively validate the classical and recent Wenzel models of wetting with high experimental precision.[1,35] In the classical Wenzel model, a key signature of the Wenzel state is that surface roughness amplifies the surface wettability.[36] Specifically, the Wenzel equation relates to the thermodynamically most stable apparent CA (θ^*) to the surface roughness, R, and the Young's CA on a flat lubricated surface, θ, and is expressed as[1,37]

$$\cos\theta^* = R\cos\theta \tag{4}$$

The Wenzel equation suggests that roughness increases surface hydrophobicity/oleophobicity for an intrinsically hydrophobic/oleophobic surface (*i.e.*, a surface on which $\theta > 90°$, according to Wenzel equation), and reduces hydrophobicity/oleophobicity for an intrinsically hydrophilic/oleophilic surface (*i.e.*, on which $\theta < 90°$).

A recent wetting model proposed by Kang and Jacobi is derived on the basis of work of adhesion, conservation equations, and surface energy minimization.[35] The Kang–Jacobi equation relates the apparent CA to the surface roughness according to

$$\frac{1-\cos\theta^* - 2\left(\frac{(2+\cos\theta^*)(1-\cos\theta^*)^2}{4}\right)^{2/3}}{\sin^2\theta^*} = R\,\frac{1-\cos\theta - 2\left(\frac{(2+\cos\theta)(1-\cos\theta)^2}{4}\right)^{2/3}}{\sin^2\theta} \tag{5}$$

The Kang–Jacobi equation is of the form $f(\theta^*) = R\cdot f(\theta)$ and captures similar physics as the Wenzel equation (*i.e.*, roughness amplifies surface wettability). However, the critical CAs for the transition of the wetting behavior are ~42° in eq 5, and 48° in Kang and Jacobi's discussion related to work of adhesion,[35] different from 90° as suggested by Wenzel equation.

To assess these two models, we systematically measured the advancing, static, and receding apparent CAs of droplets of water ($\theta = 121.3° \pm 1.1°$), ethylene glycol ($\theta = 101.6° \pm 1.4°$), hexadecane ($\theta = 70.5° \pm 1.1°$), and heptane ($\theta = 50.9° \pm 1.4°$) on the slippery rough surfaces. In addition, we verified that the CAs of these droplets were above the critical CA of Wenzel to

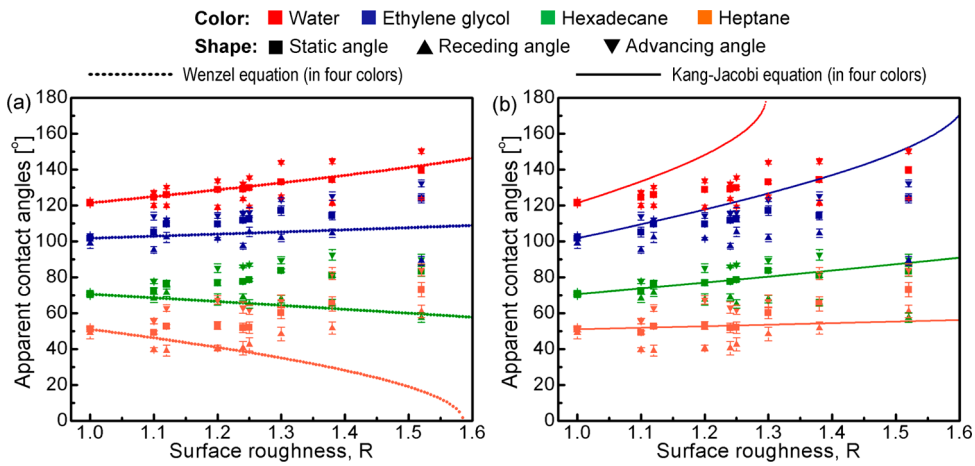

Figure 5. Comparison of the experimentally measured apparent CAs on the slippery rough surfaces with those predicted by (a) Wenzel equation and the (b) Kang–Jacobi equation. Error bars indicate standard deviations from at least three independent measurements.

hemiwicking transition, θ_h, which is given by,[38]

$$\cos\theta_h = \frac{1 - \Phi_s}{R - \Phi_s} \quad (6)$$

Specifically, when $\theta_h < \theta < \theta_c$, the droplet is in the Wenzel state; whereas when $\theta < \theta_h$, hemiwicking occurs. In addition, a previous study suggested that θ of a wetting liquid sitting on a surface with vertical microtextures should be greater than the larger value of 45° and θ_h, based on the Concus–Finn condition, in order to prevent hemiwicking from occurring.[39,40] All of our tested liquids satisfy this theoretical criterion. In all of our measurements, we did not observe the droplet leaving a wet footprint (a possible indicator for Wenzel state to hemiwicking transition) or exhibiting visible hemiwicking[38,39] on the slippery rough surfaces at the surface roughness in this study (*i.e.*, $R < 1.6$, see Supporting Information). Furthermore, we experimentally confirmed that the droplets were in the Wenzel state (Figures 3d and 4b).

Note that θ^* is bound by θ^*_A and θ^*_R (*i.e.*, $\theta^*_R \leq \theta^* \leq \theta^*_A$).[37] Therefore, validating these theoretical models would require $\Delta\theta^*$ to be much smaller than θ^*. While earlier work has attempted to experimentally validate the classical Wenzel equation,[41−43] these experiments either report measured $\Delta\theta^*$ that are on the same order of magnitude as θ^*, or do not indicate the magnitudes of $\Delta\theta^*$ that determine the possible experimental deviations from their measured θ^*. On the slippery rough surfaces, all the measured $\Delta\theta^*$ are significantly lower than θ^* (*e.g.*, $\Delta\theta^*$ for water droplets are less than 27° for $R \leq 1.52$, where $\theta \sim 121°$), indicating that the surfaces closely resemble a near-idealized rough surface.

In high CA regimes (*i.e.*, $101.6° < \theta < 121.3°$) and at moderate roughness (*i.e.*, $R < 1.6$), the predictions of the Wenzel equation are in good agreement with the measured θ^* of liquid droplets (Figure 5a), while those of the Kang–Jacobi equation overestimate the apparent contact angles (Figure 5b). In middle to low CA regimes (*e.g.*, $50.9° < \theta < 70.5°$), the Wenzel predictions start to deviate from our experimental data (*e.g.*, heptane results) (Figure 5a), but the Kang–Jacobi predictions conform closely (Figure 5b). Our experimental measurements are in contrast to the conventional concept that Wenzel equation should apply when $\theta_h < \theta < \theta_c$.[38] In addition, we observed that highly wetting liquid droplets, such as heptane, exhibit hemiwicking behaviors at high roughness (*i.e.*, $R = 2.13$)[38] as shown in Supplementary Movie S6. This indicates that the Kang–Jacobi equation may only be applicable within a certain roughness range before hemiwicking occurs.[38] Using the Krytox oil infused slippery rough surfaces, we were unable to precisely characterize the θ^* in the lower CA regime (*i.e.*, $\theta < 50.9°$) since these measurements would require the use of highly evaporative liquids (*e.g.*, pentane). Nonetheless, our experimental measurements indicate that the Wenzel and Kang–Jacobi models can only predict the apparent CAs in a certain range. Specifically, the Wenzel prediction breaks down for highly wetting liquids (*e.g.*, heptane) in the Wenzel state; whereas the Kang–Jacobi prediction fails for nonwetting liquids (*e.g.*, water).

CONCLUSIONS

In contrast to the well-established physical concept that droplets in the Cassie state are mobile and droplets in the Wenzel state are sticky,[9] our study presents the conceptually new perspective that both Cassie and Wenzel state droplets can be mobile. These new findings may inspire a new type of liquid repellent strategy for many industrial applications where enhancing droplet mobility and removal is important, particularly in applications such as liquid harvesting, condensation heat transfer, and frost prevention where the formation of Wenzel state droplets is inevitable. With a broad range of commercially available lubricants, one can select an appropriate lubricant with enhanced longevity and suitable physical or chemical characteristics

depending on specific application requirements (Supporting Information). Further application examples of the slippery rough surfaces will be described elsewhere. Note that while our work used silicon as an example, the design principle can be easily extended to other material systems such as metals, glasses, ceramics, and plastics owing to the diverse fabrication technologies available to create hierarchical surface architectures.[28,44−46] Not only is the identification of the slippery Wenzel state of technological importance, these new findings enable us to experimentally revisit the classical and recent theoretical models of wetting on rough surfaces. While both the Wenzel and Kang−Jacobi models capture the Wenzel state wetting physics within the uncertainty of our experimental data in certain CA regimes, none of these models provides a single unified theory that describes wetting physics over the whole CA and roughness spectrum where the Wenzel state exists. Our experimental characterizations motivate the search for a universal model that can capture the complete wetting physics on a rough surface. Furthermore, the discovery of the slippery Wenzel state may open up new opportunities for scientific studies related to wetting, nucleation, transport phenomena, and beyond.

METHODS

Fabrication of Nanotextured Micropillars. Square-shaped silicon micropillars were fabricated using standard photolithography and deep reactive-ion etching (DRIE) on a 4 in. ⟨100⟩ p-type silicon wafer with a thickness of 400 μm. The nanoscale grooves on every individual micropillar (Figure 3a) were formed during the DRIE process. In the DRIE process, the etching and passivation processes were enabled by two gases (SF_6, and C_4F_8, respectively) introduced in alternating cycles. The silicon substrate was etched in incremental steps, removing ∼0.7 μm in each step. First, SF_6 was injected for 7 s to etch the silicon down ∼0.7 μm; second, C_4F_8 was introduced to create a passivation layer to protect the side wall of the micropillars, preventing etching in the direction normal to the side-edges in the proceeding etch steps. These SF_6, and C_4F_8 processes were continued in alternating cycles. Each cycle leads to a "groove-like" nanostructure of height ∼30 to ∼50 nm. After the DRIE process, the photoresist on the top surfaces and polymer on the side walls of micropillars were removed by oxygen plasma. A wet etching method was used to create nanotextures on the surfaces of square micropillars. The microstructured silicon wafer obtained from the previous step was cleaned in piranha solution to remove the organics and then in 5% hydrofluoric acid (HF) solution for 20 s to remove the oxide layer. Subsequently, the wafer was immediately immersed into a solution of 4.8 M HF and 0.01 M silver nitride ($AgNO_3$) for 1 min to deposit catalysts. The Ag^+ was reduced to Ag nanoparticles, which could be deposited on the top, bottom, and side walls of the microstructured silicon surfaces. These Ag nanoparticles acted as catalysts to enhance local etching speed during the etching process. The microstructured wafer with the catalyst was put in the etching solution containing 4.8 M HF and 0.3 M hydrogen peroxide (H_2O_2) for 6 to 7 min. After the catalyst deposition and etching step, the wafer was placed into the dilute nitric acid solution to dissolve the silver dendrites. In the end, the wafer was washed with DI water and dried with nitrogen gas. Patterned nanotextured micropillars were obtained on the silicon wafer.

Silanization and Lubrication. The nanotextured silicon microstructures were silanized using heptadecafluoro-1,1,2,2- tetrahydrodecyltrichlorosilane (Gelest Inc.). These silanes were deposited onto the silicon surfaces in a vacuum chamber for 4 h. Afterward, a lubricant, such as Krytox 101 or 103 (DuPont, viscosities of 17.4 cSt and 82 cSt at 20 °C, respectively), was coated on the silanized nanotextured micropillars using a spin coater. The lubricant thickness was controlled by the spin speed of the spin coater. Higher spin speed can remove more lubricant and yield a lubricant layer that is more conformal to the micropillars. Increased spin speed helps to remove the lubricant between micropillars as shown in the environmental scanning electron microscope (ESEM) images in Figure 2.

Environmental SEM. After the lubrication process, the nanotextures were fully submerged under the lubricant layer. The lubricated micropillars were visualized by an ESEM to capture the distribution of oil lubricants on an angled stage (40° ∼ 60°). The applied voltage was 20 kV and current was 2.1 nA for the operation of ESEM. To minimize the evaporation of oil lubricants, the temperature was reduced to −5 °C before the low vacuum was applied. The pressure was set at 3.8 Torr, which is much higher than the saturation pressure of Krytox 101 at −5 °C. From the ESEM images, it is evident that at a spin speed of 3000 rpm, the lubricated bottom surface is exposed but the bottom corners are thickly covered by lubricant owing to the capillary force. However, at a spin speed of 12000 rpm, the lubricants were only retained within the nanotextures, and were completely removed from the space between micropillars. The lubricated surfaces therefore showed a surface morphology similar to that of nonlubricated micropillars. The entire surface shows patterned micropillars with a conformal lubricant layer.

Conflict of Interest: The authors declare the following competing financial interest(s): A United States provisional patent has been filed for this work.

Supporting Information Available: The Supporting Information is available free of charge on the ACS Publications website at DOI: 10.1021/acsnano.5b04151.

Further details on the design principle, wetting characteristics, longevity study, and fabrication of the slippery rough surfaces (PDF)
Wenzel droplet mobility (AVI)
Cassie droplet mobility (AVI)
Droplet mobility of a low surface tension liquid (hexadecane) in Wenzel state (AVI)
A liquid droplet maintains its mobility after the Cassie-to-Wenzel transition induced by external pressure (AVI)
A liquid droplet maintains its mobility after the Cassie-to-Wenzel transition induced by a low surface tension liquid (AVI)
Hemiwicking behavior (AVI)

Acknowledgment. The authors gratefully acknowledge the funding support by National Science Foundation (NSF) CAREER Award No.: 1351462 (cross-species materials & wetting science) and Office of Naval Research MURI Award No.: N00014-12-1-0875 (materials fabrication). Stogin acknowledges the support from the NSF Graduate Research Fellowship (Grant No. DGE1255832). Part of the work was conducted at the Penn State node of the NSF-funded National Nanotechnology of Infrastructure Network.

REFERENCES AND NOTES

1. Wenzel, R. N. Resistance of Solid Surfaces to Wetting by Water. *Ind. Eng. Chem.* **1936**, *28*, 988–994.
2. Cassie, A. B. D.; Baxter, S. Wettability of Porous Surfaces. *Trans. Faraday Soc.* **1944**, *40*, 546–550.
3. Tuteja, A.; Choi, W.; Ma, M.; Mabry, J. M.; Mazzella, S. A.; Rutledge, G. C.; McKinley, G. H.; Cohen, R. E. Designing Superoleophobic Surfaces. *Science* **2007**, *318*, 1618–1622.
4. Quere, D. Wetting and Roughness. *Annu. Rev. Mater. Res.* **2008**, *38*, 71–99.

5. Wong, T.-S.; Kang, S. H.; Tang, S. K. Y.; Smythe, E. J.; Hatton, B. D.; Grinthal, A.; Aizenberg, J. Bioinspired Self-Repairing Slippery Surfaces with Pressure-Stable Omniphobicity. *Nature* **2011**, *477*, 443–447.
6. Deng, X.; Mammen, L.; Butt, H.-J.; Vollmer, D. Candle Soot as a Template for a Transparent Robust Superamphiphobic Coating. *Science* **2012**, *335*, 67–70.
7. Wong, T. S.; Sun, T. L.; Feng, L.; Aizenberg, J. Interfacial Materials with Special Wettability. *MRS Bull.* **2013**, *38*, 366–371.
8. Liu, T.; Kim, C.-J. Turning a Surface Superrepellent even to Completely Wetting Liquids. *Science* **2014**, *346*, 1096–1100.
9. Lafuma, A.; Quere, D. Superhydrophobic States. *Nat. Mater.* **2003**, *2*, 457–460.
10. Patankar, N. A. Transition between Superhydrophobic States on Rough Surfaces. *Langmuir* **2004**, *20*, 7097–7102.
11. Gibbs, J. W. *The Scientific Papers of J. Willard Gibbs*; Dover Publications: New York, 1961.
12. Oliver, J. F.; Huh, C.; Mason, S. G. Resistance to Spreading of Liquids by Sharp Edges. *J. Colloid Interface Sci.* **1977**, *59*, 568–581.
13. Koishi, T.; Yasuoka, K.; Fujikawa, S.; Zeng, X. C. Measurement of Contact-Angle Hysteresis for Droplets on Nanopillared Surface and in the Cassie and Wenzel States: A Molecular Dynamics Simulation Study. *ACS Nano* **2011**, *5*, 6834–6842.
14. Wong, T.-S.; Huang, A. P.-H.; Ho, C.-M. Wetting Behaviors of Individual Nanostructures. *Langmuir* **2009**, *25*, 6599–6603.
15. Poetes, R.; Holtzmann, K.; Franze, K.; Steiner, U. Metastable Underwater Superhydrophobicity. *Phys. Rev. Lett.* **2010**, *105*, 166104.
16. Daniel, D.; Mankin, M. N.; Belisle, R. A.; Wong, T.-S.; Aizenberg, J. Lubricant-Infused Micro/Nano-Structured Surfaces with Tunable Dynamic Omniphobicity at High Temperatures. *Appl. Phys. Lett.* **2013**, *102*, 231603.
17. Tuteja, A.; Choi, W.; Mabry, J. M.; McKinley, G. H.; Cohen, R. E. Robust Omniphobic Surfaces. *Proc. Natl. Acad. Sci. U. S. A.* **2008**, *105*, 18200–18205.
18. Bai, H.; Wang, L.; Ju, J.; Sun, R.; Zheng, Y.; Jiang, L. Efficient Water Collection on Integrative Bioinspired Surfaces with Star-Shaped Wettability Patterns. *Adv. Mater.* **2014**, *26*, 5025–5030.
19. Miljkovic, N.; Enright, R.; Nam, Y.; Lopez, K.; Dou, N.; Sack, J.; Wang, E. N. Jumping-Droplet-Enhanced Condensation on Scalable Superhydrophobic Nanostructured Surfaces. *Nano Lett.* **2013**, *13*, 179–187.
20. Hou, Y.; Yu, M.; Chen, X.; Wang, Z.; Yao, S. Recurrent Filmwise and Dropwise Condensation on a Beetle Mimetic Surface. *ACS Nano* **2015**, *9*, 71–81.
21. Varanasi, K. K.; Deng, T.; Smith, J. D.; Hsu, M.; Bhate, N. Frost Formation and Ice Adhesion on Superhydrophobic Surfaces. *Appl. Phys. Lett.* **2010**, *97*, 234102.
22. Lee, C.; Kim, C.-J. Underwater Restoration and Retention of Gases on Superhydrophobic Surfaces for Drag Reduction. *Phys. Rev. Lett.* **2011**, *106*, 014502.
23. Boreyko, J.; Chen, C.-H. Restoring Superhydrophobicity of Lotus Leaves with Vibration-Induced Dewetting. *Phys. Rev. Lett.* **2009**, *103*, 174502.
24. Adera, S.; Raj, R.; Enright, R.; Wang, E. N. Non-Wetting Droplets on Hot Superhydrophilic Surfaces. *Nat. Commun.* **2013**, *4*, 2518.
25. Johnson, R. E.; Dettre, R. H. Contact Angle Hysteresis. III. Study of an Idealized Heterogeneous Surface. *J. Phys. Chem.* **1964**, *68*, 1744–1750.
26. Lafuma, A.; Quéré, D. Slippery Pre-Suffused Surfaces. *Europhys. Lett.* **2011**, *96*, 56001.
27. Nishino, T.; Meguro, M.; Nakamae, K.; Matsushita, M.; Ueda, Y. The Lowest Surface Free Energy Based on -CF3 Alignment. *Langmuir* **1999**, *15*, 4321–4323.
28. Kim, P.; Kreder, M. J.; Alvarenga, J.; Aizenberg, J. Hierarchical or Not? Effect of the Length Scale and Hierarchy of the Surface Roughness on Omniphobicity of Lubricant-Infused Substrates. *Nano Lett.* **2013**, *13*, 1793–1799.
29. Furmidge, C. G. L. Studies at phase interfaces. I. The Sliding of Liquid Drops on Solid Surfaces and a Theory for Spray Retention. *J. Colloid Sci.* **1962**, *17*, 309–324.
30. Chen, W.; Fadeev, A. Y.; Hsieh, M. C.; Öner, D.; Youngblood, J.; McCarthy, T. J. Ultrahydrophobic and Ultralyophobic Surfaces: Some Comments and Examples. *Langmuir* **1999**, *15*, 3395–3399.
31. Fadeev, A. Y.; McCarthy, T. J. Trialkylsilane Monolayers Covalently Attached to Silicon Surfaces: Wettability Studies Indicating that Molecular Topography Contributes to Contact Angle Hysteresis. *Langmuir* **1999**, *15*, 3759–3766.
32. Gao, L.; McCarthy, T. J. Contact Angle Hysteresis Explained. *Langmuir* **2006**, *22*, 6234–6237.
33. Liu, M.; Zheng, Y.; Zhai, J.; Jiang, L. Bioinspired Super-antiwetting Interfaces with Special Liquid-Solid Adhesion. *Acc. Chem. Res.* **2010**, *43*, 368–377.
34. Luo, C.; Xiang, M. Angle Inequality for Judging the Transition from Cassie−Baxter to Wenzel States When a Water Drop Contacts Bottoms of Grooves between Micropillars. *Langmuir* **2012**, *28*, 13636–13642.
35. Kang, H. C.; Jacobi, A. M. Equilibrium Contact Angles of Liquid Droplets on Ideal Rough Solids. *Langmuir* **2011**, *27*, 14910–14918.
36. Wenzel, R. N. Surface Roughness and Contact Angle. *J. Phys. Colloid Chem.* **1949**, *53*, 1466–1467.
37. Marmur, A. Solid-Surface Characterization by Wetting. *Annu. Rev. Mater. Res.* **2009**, *39*, 473–489.
38. Bico, J.; Thiele, U.; Quéré, D. Wetting of Textured Surfaces. *Colloids Surf., A* **2002**, *206*, 41–46.
39. Garg, V.; Qiao, L.; Sarwate, P.; Luo, C. Creation of Superwetting Surfaces with Roughness Structures. *Langmuir* **2014**, *30*, 14469–14475.
40. Concus, P.; Finn, R. On the Behavior of a Capillary Surface in a Wedge. *Proc. Natl. Acad. Sci. U. S. A.* **1969**, *63*, 292–299.
41. Jung, Y. C.; Bhushan, B. Dynamic Effects Induced Transition of Droplets on Biomimetic Superhydrophobic Surfaces. *Langmuir* **2009**, *25*, 9208–9218.
42. Yoshimitsu, Z.; Nakajima, A.; Watanabe, T.; Hashimoto, K. Effects of Surface Structure on the Hydrophobicity and Sliding Behavior of Water Droplets. *Langmuir* **2002**, *18*, 5818–5822.
43. Koch, B. M. L.; Amirfazli, A.; Elliott, J. A. W. Wetting of Rough Surfaces by a Low Surface Tension Liquid. *J. Phys. Chem. C* **2014**, *118*, 23777–23782.
44. Erbil, H. Y.; Demirel, A. L.; Avci, Y.; Mert, O. Transformation of a Simple Plastic into a Superhydrophobic Surface. *Science* **2003**, *299*, 1377–1380.
45. Azimi, G.; Dhiman, R.; Kwon, H.-M.; Paxson, A. T.; Varanasi, K. K. Hydrophobicity of Rare-Earth Oxide Ceramics. *Nat. Mater.* **2013**, *12*, 315–320.
46. Wang, N.; Xiong, D.; Deng, Y.; Shi, Y.; Wang, K. Mechanically Robust Superhydrophobic Steel Surface with Anti-Icing, UV-Durability, and Corrosion Resistance Properties. *ACS Appl. Mater. Interfaces* **2015**, *7*, 6260–6272.